Energy Science & Engineering

MODELLING AND ANALYSIS OPEN ACCESS

Optimization Simulation of Mooring System of Floating Offshore Wind Turbine Platform Based on SPH Method

Weibo Du | Peigang Jiao | Kangning Li | Jiaming Ding

College of Mechanical Engineering, Shandong Jiaotong University, Jinan, China

Correspondence: Peigang Jiao (jiaopeigang@163.com)

Received: 29 May 2024 | **Revised:** 14 September 2024 | **Accepted:** 2 October 2024

Funding: This research was supported by Research Project on Key Technologies for the Development of All-Terrain Intelligent Orchard Platform (2019GNC106032).

Keywords: floating offshore wind turbine | mooring system simulation | solid–liquid coupling | SPH method

ABSTRACT

In this paper, the Smoothed Particle Hydrodynamics method is used to simulate the dynamic response of the floating offshore wind turbine mooring system in a complex marine environment by using its advantages of dealing with free surface flow and fluid–structure interaction. The single-cable mooring system and the double-cable mooring system are introduced into the numerical simulation model of fluid–solid coupling interaction. The first-order irregular wave and the second-order regular wave are used to simulate different wave conditions. The operating state of the platform in these two cases is analyzed, and the accurate data such as the velocity change of the geometric center of the platform and the change of six degrees of freedom are obtained. Using visual processing and data analysis, it is found that the optimized double-cable mooring system structure improves the vibration reduction ability of the platform.

1 | Introduction

In the face of the global energy crisis and environmental changes, the development and utilization of renewable energy has become one of the key research directions in the world. As a clean and efficient energy acquisition method, offshore wind power generation has received extensive attention and rapid development [1, 2]. In particular, floating offshore wind power generation technology has a broader application prospect because it is not limited by water depth and can be installed in deep water areas. However, the stability and reliability of the floating wind turbine greatly depend on the design and performance of its mooring system, which requires accurate prediction and analysis of its dynamic response in complex marine environments.

As a meshless method, Smoothed Particle Hydrodynamics (SPH) method has become a powerful tool for analyzing the response of floating structures due to its advantages in dealing with free surface flow [3] and fluid–structure interaction [4]. On the basis of the SPH method, the simulation of the mooring system of the floating offshore wind turbine [5] can not only capture the hydrodynamic behavior in the complex marine environment, but also simulate the influence of the wave load on the floating structure and the dynamic characteristics of different mooring systems under different wave loads.

Aslami et al. have introduced a fully coupled model of three-dimensional (3D) debris motion in shallow-water flow, and uses SPH to solve the shallow-water equations [6].

Capasso et al. have used the SPH meshless method to study the dynamics of planar hull under regular head waves, and the experimental results under different wave conditions have

[Correction added on 13 December 2024, after first online publication: the corresponding authors is changed.]

verified the feasibility of the method, which is in good agreement with the experimental results in general [7].

Barreiro et al. have proposed a new implementation to simulate the behavior of moored lines is presented for SPH models. This new approach allows reproducing the forces on floating bodies and other off shore structures moored to the seabed [8].

Tagliafierro et al. have defined a complete numerical environment for simulating interactions of floating structures to assess the quality of fluid–solid interactions, as well as conventional wave tests [9], and uses SPH method to determine and simulate a tightly mooring point absorbing wave energy converter and its inherent power output device [10]. Then, based on the DeepCwind offshore wind semisubmersible concept moored with a system of taut-lines and tested for free-decay surge and heave motion [11].

Quartier has conducted studies to test and extend the applicability of SPH in modeling wave energy converter and anchored floating structures, and has taken the necessary steps to optimize GEC designs and reduce their costs [12].

In this paper, the research progress of mooring system simulation of floating offshore wind turbine platform based on the SPH method is studied. On the basis of the basic principle of the SPH method and its application in the field of marine engineering [9, 13], especially its advantages in simulating fluid–structure interaction, the SPH method is applied to the simulation process of the mooring system of floating offshore wind turbine platform, including key technical problems, such as model establishment, boundary condition processing, and mooring line model integration. By simulating the dynamic response of mooring system platforms with two different structures of the single-cable mooring system and the double-cable mooring system under different wave conditions, and analyzing the subsequent visualization and data processing, the SPH method is demonstrated. The ability to simulate the mooring system of the floating wind turbine platform, as well as the ability to optimize the design of the mooring system and improve the stability and reliability of the floating wind turbine. Through continuous technological innovation and optimization, the challenges faced by the simulation based on the SPH method in the future development of floating offshore wind power technology are solved [14]. It includes research directions such as improving simulation accuracy, reducing computational costs, adapting to more complex marine environments, and its potential impact on promoting the commercialization process of offshore wind power technology [15], providing strong support for the development of offshore wind power technology.

The rest of this article is composed as follows. First, the SPH method and its application are introduced, including the coupling with MoorDyn and the realization of related formulas. Second, the model structure design used in this paper is described, and the corresponding numerical model is established. Subsequently, the numerical results are analyzed and their consistency with the experimental results is tested, including the simulation values of geometric center change, buoyancy change and velocity change. Finally, the conclusion part summarizes this article.

2 | SPH Method

The SPH method is a particle-based computational fluid dynamics simulation method. Since it was proposed by Lucy [16] and Gingold and Monaghan in 1977 [17], it has developed into a powerful tool for dealing with complex free surface flows [3] and nonlinear fluid problems. The core idea of the SPH method is to represent the fluid in the fluid domain as a series of discrete particles. Through these particles and their interactions, the SPH method can simulate the macroscopic behavior of the fluid. The SPH method is very suitable for simulating fluid problems with complex geometric boundaries and free surfaces. Compared with the traditional Finite Volume Method and Finite Element Method, the SPH method has many advantages, such as no need for grids, can deal with complex boundaries and deformed fluids, and can adaptively change the particle density. The two main characteristics of the SPH method are Lagrangian and meshless. These characteristics determine that the SPH method has obvious advantages over the traditional mesh-based method in the study of strong convection, large deformation, and moving boundary problems [18]. In this paper, the dynamic response of mooring system platforms with different structures under different wave conditions is simulated by establishing the mooring system simulation of floating offshore wind turbine, which provides theoretical support for the design and optimization of the mooring system of floating offshore wind turbine platform in the future.

2.1 | Coupling of SPH Method With MoorDyn

The mooring system is a common structure in ocean engineering, which is used to limit the position of ships or offshore platforms in specific waters. These systems usually include components, such as anchor chains, cables, floating bodies, and so forth, and their design and analysis need to take into account complex marine environmental factors, such as waves, currents, wind, and so forth. In the field of ocean engineering, considering the complex interaction between waves, fluids and structures, the coupling of the SPH method and MoorDyn provides a powerful analysis method in mooring system analysis [5]. By dividing the fluid into a series of particles with a certain mass and volume, and simulating the motion and interaction of these particles, the SPH method can capture the hydrodynamic behavior at the micro level. It can not only simulate complex phenomena such as free surface of the fluid and wave strike, but also deal with the interaction between the fluid and the structure, such as the impact force and drag force of the fluid on the mooring line. MoorDyn discretizes the mooring line into point masses (nodes), which are connected by linear spring damper segments to provide axial elasticity. By coupling the SPH method with MoorDyn, a more accurate simulation of mooring system behavior in complex marine environments can be realized.

Coupling the SPH method with MoorDyn [19, 20] can achieve a more accurate simulation of the behavior of the mooring system in a complex marine environment. The kinematics of the guide cable is transferred to MoorDyn to calculate the dynamics of the mooring system in multiple time steps, and then the obtained tension vector of the guide cable is transferred back to the SPH method, as shown in Figure 1. In the coupling analysis, the structural response and hydrodynamic effect of the mooring system are solved at the same

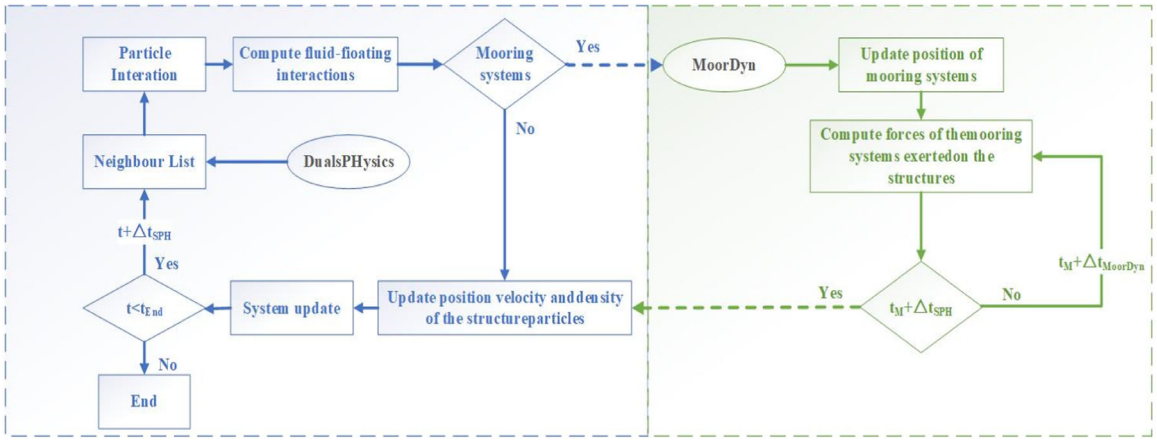

FIGURE 1 | Coupling diagram of Smoothed Particle Hydrodynamics method and MoorDyn. Figure 1 shows the coupling of DualSPHysics–MoorDyn, where the guide hook kinematics is passed to MoorDyn to calculate the mooring system dynamics for one or more time steps, and then the resulting guide hook tension vector is transmitted back for coupling to achieve a more accurate simulation of the mooring system behavior in complex ocean environments.

time. The influence of hydrodynamic factors on the performance of the mooring system can be obtained, such as the tension change of the anchor chain and the motion response of the floating body. The motion and rotation (V, Ω, R_0) of the initial solution of the platform are transmitted to MoorDyn and used as the input of the mooring line kinematics. Then MoorDyn solves the mooring line behavior within the time step used in the model, calculates the force at the junction of the guide cable $(dV/dt, d\Omega/dt)$, and transmits it back. Finally, the surplus force calculated in the previous step is used to obtain the final force acting on the platform, which is used to calculate the final motion and rotation of the platform.

2.2 | Calculation Method

In the SPH method, the computational domain is described by a set of particles, each of which constitutes the basic computational unit of the field variable approximation. These particles each carry unique material properties, such as mass and density. They move according to the equations controlled by the law of conservation based on the influence of internal and external forces. In the fluid dynamics simulation, according to the physical properties of the surrounding particles, the discrete Navier–Stokes equations [21, 22] are locally integrated at the position of each particle. The set of adjacent particles is determined by a distance-based function, which can be two-dimensional (2D) or 3D, and the characteristic length or smooth length is denoted by h [23].

2.2.1 | SPH Particle Approximation

The construction of the SPH equation is first to use the smooth function approximation method of integral representation function, and then to integrate any function step by step, and then to approximate the integral expression of the function by the sum of the values of the nearest adjacent particles [24]. In the SPH method, any function in the continuous variable field, such as density, mass, energy, temperature, and so forth, can be written as the product of the function $F(r)$ and a smooth function $W(r - r', h)$:

$$F(r) = \int_{\Omega} F(r') W(r - r', h)\, dr'. \tag{1}$$

In the formula, r is the position vector, Ω is the integral interval of r, $W(r - r', h)$ is the smooth function, h is the yellow smooth length, and the smooth function W should satisfy the following conditions: normalization, nonnegativity, attenuation, symmetry, smoothness, and compact support [25]. When $F(r)$ is defined and continuous on Ω, the integral representation used in (1) is exact.

In the SPH method, the whole computational problem domain can be represented by finite particles, which have independent mass and occupy independent space. The continuous integral expression (1) in SPH smooth function approximation is transformed into a discretization form, and the discretization process of particle superposition summation is the particle approximation method.

In the discrete representation, the function at particle i can be expressed as

$$F(r) \equiv \sum_j F(r_j) \frac{m_j}{\rho_j} W_{ij}, \tag{2}$$

where ρ_j is the density of particle j ($j = 1, 2, ..., N$), where N is the total number of particles in the support domain of particle j, m_j is the mass of particle j, such that the volume of particle j is $V_j = m_j/\rho_j$ and $W(r_i - r_j, h)$ is a smooth function.

In the SPH method, selecting the appropriate kernel function is very important for the effective approximation of the discrete point set. This choice not only affects the size of the particle action range under the function definition, but also directly affects the consistency between the kernel function approximation and the particle approximation and the accuracy of the overall calculation. In this paper, the Wendland kernel function

is adopted, and the Wendland function has better smoothness and differentiability [26].

$$W(r,h) = \alpha_D\left(1-\frac{q}{2}\right)^4(2q+1), \quad 0 \le q \le 2, \tag{3}$$

where α_D is applied to two-dimensional $7/4\pi h^2$, three-dimensional $21/16\pi h^3$, q is the relative length, $q = r/h$.

2.2.2 | Control Equations

The Navier–Stokes governing equations [21, 22] are discretized by introducing the particle approximation method in the SPH form. In the Lagrangian form, the momentum equation and the continuity equation can be discretized as

$$\frac{d\mathbf{v}_a}{dt} = -\sum_b m_b\left(\frac{P_b + P_a}{\rho_b \cdot \rho_a} + \Pi_{ab}\right)\nabla_a W_{ab} + g, \tag{4}$$

$$\frac{d\rho_a}{dt} = \rho_a \sum_b \frac{m_b}{\rho_b} \mathrm{v}_{ab} \cdot \nabla_a W_{ab}, \tag{5}$$

where Γ is the dissipative term and g is the gravitational acceleration, P_k and ρ_k are the pressure and density that correspond to particle k. The specific form of the viscosity term Π_{ab} is

$$\Pi_{ab} = \begin{cases} \frac{-\alpha\overline{c_{ab}}\mu_{ab}}{\overline{\rho_{ab}}}, & v_{ab} \cdot r_{ab} < 0, \\ 0, & v_{ab} \cdot r_{ab} > 0, \end{cases} \tag{6}$$

where $\mathrm{r}_{ab} = r_a - r_b$, $v_{ab} = v_a - v_b$, r_k, and v_k represent the position vector and velocity vector of particle k, respectively, α is the viscosity coefficient, which can be adjusted as needed to reduce the numerical dissipation, wave propagation, and wave load on coastal structures. Altomare et al. have shown that setting the viscosity coefficient to 0.01 can obtain the optimal simulation results [27, 28]. Where $\mu_{ab} = hv_{ab} \cdot r_{ab}/(r_{ab}^2 + \eta^2)$, $\eta^2 = 0.01h^2$, $\overline{c_{ab}} = 0.5(c_a + c_b)$, $\overline{c_{ab}}$ is the average speed of sound.

According to the method of Peng et al. [29], the fluid is regarded as a weakly compressible fluid in the SPH form, and the equation of state is used to describe the relationship between fluid pressure and density, which is expressed as

$$P = B\left[\left(\frac{\rho}{\rho_0}\right)^\gamma - 1\right] \tag{7}$$

for γ is a constant, generally take 7, $B = c_0^2\rho_0/\gamma$; $\rho_0 = 1000\,\mathrm{kg/m^3}$ is the reference density, and $c_0 = c(\rho_0) = \sqrt{\partial P/\partial\rho}$ is the sound velocity related to the reference density.

When calculating the motion of a floating body driven by waves and mooring lines, by assuming that the body is rigid [30], the net force on each boundary particle is computed according to the sum of the contributions of all surrounding fluid particles according to the designated kernel function and smoothing length. Each boundary particle k therefore experiences a force f_k per unit mass given by

$$f_k = \sum_{a \in WP_s} f_{ka}, \tag{8}$$

where f_{ka} is the force per unit mass exerted by the fluid particle a on the boundary particle k, which is given by

$$m_k f_{ka} = -m_a f_{ak}. \tag{9}$$

For the motion of the moving body, the basic equations of rigid body dynamics can then be used:

$$M\frac{dV}{dt} = \sum_{k \in BP_s} m_k f_k, \tag{10}$$

$$I\frac{d\Omega}{dt} = \sum_{k \in BP_s} m_k(r_k - R_0) \times f_k, \tag{11}$$

where m_k is the mass of particle k, m_a is the mass of particle a, M is the mass of the floating body, V is the velocity of the floating body, BP_s is the boundary particle of the floating body, I is inertial force, Ω is the rotation speed of the floating body, and R_0 is the position of the center of gravity. Each boundary particle within the body then has a velocity given by

$$u_k = V + \Omega \times (r_k - R_0). \tag{12}$$

Finally, the boundary particles within the rigid body are moved by integrating Equation (12) in time.

2.2.3 | Boundary Conditions

The weakly compressible SPH method can directly satisfy the free surface boundary conditions, and the treatment of the wall boundary conditions directly affects the solution accuracy of the whole flow field. Therefore, it is very important to correctly handle the wall boundary conditions for the solution accuracy. In this paper, the dynamic boundary condition (DBC) [31] is used. The DBC is the default method used in DualSPHysics. The boundary particles are regarded as fluid particles, which satisfies the same equation as the method, but they do not move like fluid particles. Instead, they are either kept in a fixed position or moved in a man-made way. Compared with other boundary conditions, this is an important advantage, especially for simulating practical engineering problems.

3 | Numerical Model Design

3.1 | Numerical Model

The mooring system of the floating offshore wind turbine is mainly composed of multiple sets of cable systems. These cable systems are distributed around the floating wind turbine and connect the wind turbine to the seabed [32]. The numerical model of this experiment has a 3D model diagram and a 3D model particle diagram. As shown in Figures 2 and 3, the flume is 4.7 m long, 0.4 m wide, and the water depth is 0.3 m. The wave maker is set on the left side of

FIGURE 2 | Three-dimensional (3D) model of numerical model. Figure 2 is the 3D model diagram of the numerical model of this experiment. The length of the tank is 4.7 m, the width is 0.4 m, the water depth is 0.3 m, and a wave generator is set on the left side of the tank to simulate the wave environment.

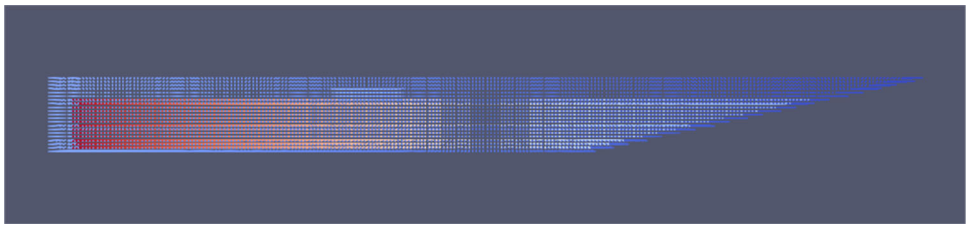

FIGURE 3 | Numerical model three-dimensional (3D) model particle diagram. Figure 3 is the numerical model of this experiment, and the 3D model particle diagram after visualization using Praview software.

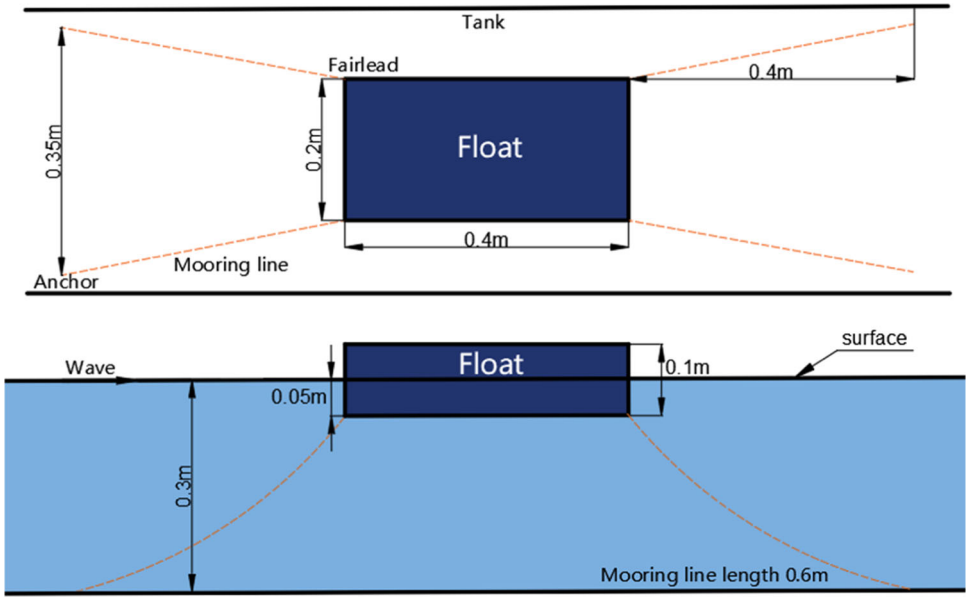

FIGURE 4 | Schematic diagram of the single-ropeway mooring system. Figure 4 shows the connection mode of the single-cable mooring system in this experiment. The upper end of the mooring line is connected to the top of the base of the platform, and the lower end is fixed on the sea floor. From the top view, all four mooring lines are connected to the top of the base of the platform and are in a catenoid state under a certain pretension.

the flume to simulate the wave environment, and the wave elimination device is set on the right side.

3.2 | The Single-Cable Mooring System

The mooring system used in this paper is composed of multiple "Lines" type mooring line units. These units are constructed by the segmentation method, and a cable is split into 20 equal-sized line segments, connecting 21 nodes. In the single-cable mooring system, the upper end of the mooring line is connected to the top of the base of the platform, and the lower end is fixed on the seabed. From the top view, the four mooring lines are connected to the top of the base of the platform and are in a catenary state under a certain pretension, as shown in Figure 4.

3.3 | The Double-Cable Mooring System

To study the influence of different mooring systems on the platform shaking of floating offshore wind turbines, this paper mainly innovates the structural form of the mooring system and proposes a double-cable mooring system. In the double-cable mooring system, the main cable and the auxiliary cable are still composed of multiple "Lines" type mooring line units. These units are constructed by the segmentation method, and a cable is split into 20 equal-sized segments, connecting 21 nodes. The main mooring line setting is the same as the mooring line parameters in the single-cableway mooring system. The upper end of the secondary mooring line is connected to the platform wall, and the lower end is connected to the seabed surface. The four secondary mooring lines on the side view are connected at 0.025 m above the main mooring line and are in a catenary state under a certain pretension, as shown in Figure 5.

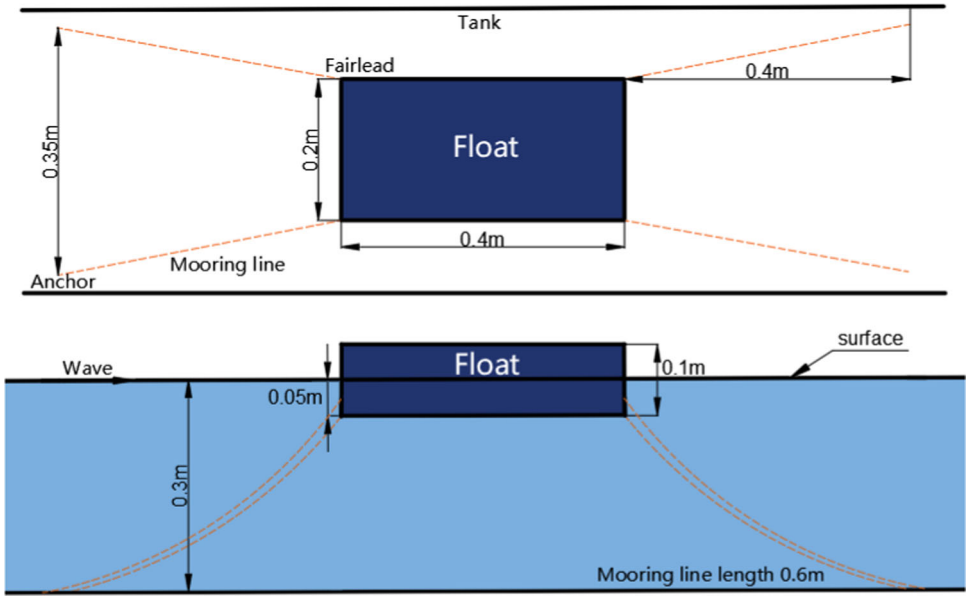

FIGURE 5 | Schematic diagram of the double-ropeway mooring system. Figure 5 shows the connection mode of the double-cable mooring system in this experiment. The upper end of the main mooring line is connected to the top of the base of the platform, the lower end is fixed on the seabed, the upper end of the auxiliary mooring line is connected to the wall of the platform, and the lower end is connected to the sea floor. In the side view, the four auxiliary mooring lines are connected to 0.025 m above the main mooring line and are in the state of catenation under certain pretension.

The SPH method is used to study the dynamic response of the offshore floating wind turbine platform under the action of waves after the installation of the double-cable mooring system. It is compared with the dynamic response of the offshore floating wind turbine installed with the original single-cable mooring system under the same environmental conditions to verify its vibration reduction performance. To make the numerical results more accurate, the simulation time of 20 s is divided into 400 steps.

3.4 | Platform Six Degrees of Freedom

The stability of a floating offshore wind turbine platform has an important influence on its wind energy conversion efficiency. The mooring system with better stability can keep the platform in a relatively fixed position under wave and flow conditions, and show a smaller floating speed, which can better improve the stability and power generation efficiency of the whole generator system, The floating amplitude of the platform directly affects its stability. The floating offshore wind turbine platform has six degrees of freedom of motion, including translation along the *x*-, *y*-, and *z*-axes and rotation around each axis [33]. The horizontal oscillation includes sway, surge, and heave, and its size is expressed by the length unit *m*. Rotation includes roll, pitch, and yaw, and its strength is represented by the angle unit rad. The motion of the platform on six degrees of freedom is shown in Figure 6.

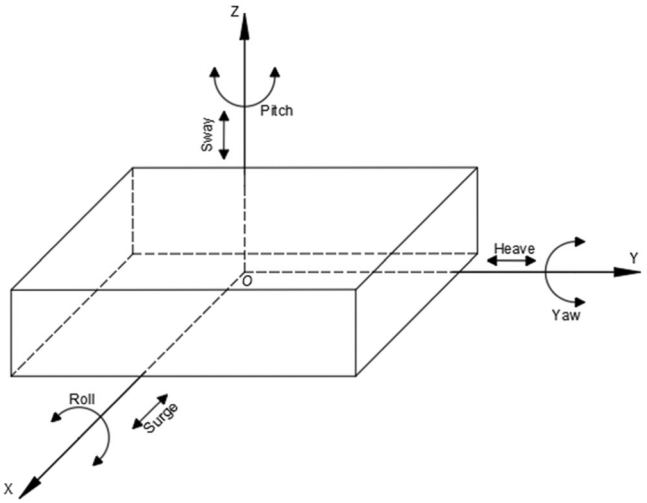

FIGURE 6 | Motion freedom diagram of floating offshore wind turbine platform. Figure 6 shows the movement of floating offshore wind turbine platform with six degrees of freedom, including translation along the *x*-, *y*-, and *z*- axes and rotation around each axis. Translation includes sway, surge, and heave. Rotation includes roll, pitch, and yaw.

3.5 | The Influence of the Double-Cable Mooring System on Platform Stability

The double-cable mooring system has shown a significant improvement in the translational and rotational stability of the platform through multipoint support, torque distribution, dynamic adjustment, and redundancy design. Compared with the single-cable mooring system, the improvement of platform stability of the double-cable mooring system is mainly reflected in the comprehensive advantages of translation and rotation control. This system can not only effectively control the lateral displacement and rotation amplitude of the platform, but also maintain high-precision positioning and stability in complex marine environments.

The single-cable mooring system adopts a single-point fixed platform. In the face of complex sea conditions, the platform is prone to large lateral displacement and rotation. In contrast, the double-cable mooring system forms a double-point support structure by adding a mooring point on one side, which improves the stability of

the platform in many aspects. In terms of translational stability, the double-cable mooring system provides the platform with multi-directional stability through two cables. When subjected to wave loads, the force can be more evenly distributed on the two cables, reducing the floating (translational) amplitude of the platform, inhibiting the swing of the platform on three degrees of freedom, and reducing the stress concentration on a single cable. To prevent the cable from breaking due to excessive pressure on the cable; in terms of rotational stability, the double-cable mooring system improves the resistance of the platform to rotational motion by increasing the mooring points, and the two mooring points can effectively disperse and resist the rotational torque from the wind and waves, and constrain the platform in multiple directions, thereby reducing the platform. The swing (rotation) amplitude reduces the amplitude and frequency of the platform's rotation when it is subjected to wave loads.

On the other hand, when one cable of the double-cable mooring system breaks or fails, the other cable can still provide certain support, slow down the process of platform instability, and reduce the risk of platform out of control due to a single-cable failure.

4 | Numerical Results Analysis

In this paper, the structure of the mooring system of the floating offshore wind turbine platform is innovated to explore how to optimize the structure of the mooring system and improve its vibration reduction performance. The SPH code and DualSPHysics are used to simulate the mooring system of the platform [34].

4.1 | Numerical Parameter Selection

The time integration scheme uses the Symplectic method [35], which is second-order accurate in time. It is an ideal choice for the Lagrangian scheme because it is time reversible and symmetrical without maintaining the geometric characteristic diffusion term. Since the effectiveness of the SPH code and the improved algorithm has been proved in the wide application of free-form surfaces, moving interfaces, and fluid–solid interactions, it is used to study the mooring system structure. The simulation structure parameters are shown in Table 1.

4.2 | Pressure Verification

The SPH method usually assumes that the fluid is ideal, that is, incompressible and nonviscous. However, in practical applications, the fluid usually has certain compressibility and viscosity. Therefore, the pressure field in the actual simulation may show different characteristics. It is necessary to verify that the simulation experiment is consistent with the actual physical properties, so as to avoid the phenomenon of abnormal pressure oscillation or negative pressure in the local area due to the fluctuation of the particles. Through verification, it can be ensured that the distribution of the pressure field under different particle spacing is reasonable, which can not only capture local details, but also maintain global physical consistency and ensure the accuracy of the overall results. A simple tank was established with reference to Fatehi and Manzari [36] to verify the static pressure of the fluid, and the theoretical pressure of the water depth of 0.2–0.6 m was solved according to the state equation of Equation (7) and compared with the simulated pressure.

TABLE 1 | Structure parameter table.

Process	Options
Dimension	3D
Domain (m)	5 * 1 * 1
Kernel function	Wendland
Time integration	Symplectic
Viscosity	Artificial
Boundary	DBC
Simulation time (s)	20
Initial particle distance (m)	0.02
h (m)	0.0392
Fluid particles	59,614
Boundary particle	1142

Abbreviation: DBC, dynamic boundary condition.

By comparing the numerical results with the experimental results, Figure 7 uses DualSPHysics to obtain the values of three different particle spacings ($dp = 0.01$ m, $dp = 0.02$ m, $dp = 0.03$ m). By reducing the particle spacing and refining the number of simulated particles, it is proved that the numerical results converge to the experimental data to ensure the rationality and reliability of the SPH method simulation results [5].

4.3 | Variation of Geometric Center of Floating Offshore Wind Turbine Platform

To verify the convergence of the SPH method, five different initial particle spacings were set up in this study, which were 0.05, 0.03, 0.02, 0.015, and 0.01 [26]. The nearest neighbor particle search method used in this paper is the list search algorithm. Smaller particle spacing will have better calculation accuracy, but at the same time, more particles will be needed to reduce the calculation efficiency. The calculation time per 1000 steps in the whole calculation process is taken as the average calculation efficiency. As the particle spacing gradually decreases, the number of particles required for calculation gradually increases, and the average calculation efficiency gradually increases. Mao et al. [37] When the gradient field in the entire problem domain is quite different, we can use a smaller spacing ratio in the region with a larger gradient and use a larger spacing ratio in the region with a smaller gradient of the variable, thereby saving computational costs. Table 2 shows the average calculation time of each 1000 steps in the whole calculation process with different particle spacings. To ensure the experimental accuracy and computational efficiency, an initial particle spacing of 0.02 was selected in this study.

Through the comparison between the experiment and the numerical simulation experiment (Figure 8), it is found that the center variation amplitude of the single-cable mooring system in the numerical simulation is basically consistent with the

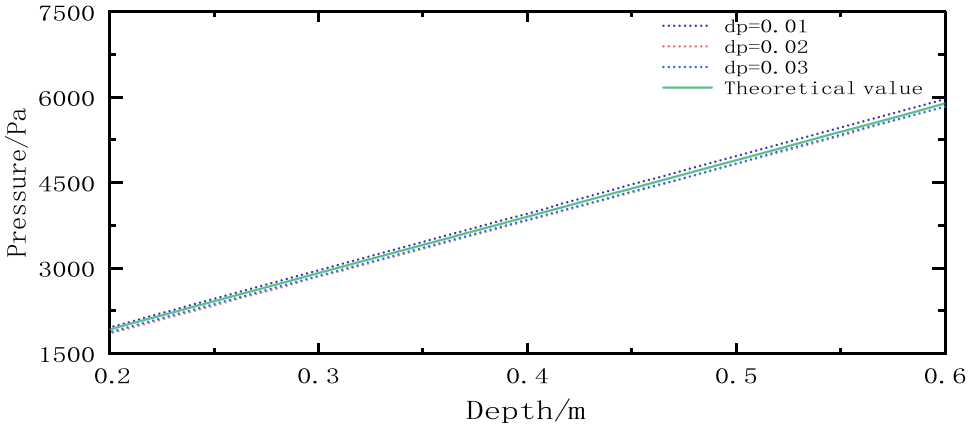

FIGURE 7 | Theoretical pressure and simulated pressure in water depth of 0.2–0.6 m. Figure 7 refers to Fatehi et al. to establish a simple storage tank for fluid static pressure verification and solve the theoretical pressure of 0.2–0.6 m in water depth according to the state equation and compare it with the simulated pressure to verify the rationality of the pressure field in this simulated experiment.

TABLE 2 | The average calculation time per 1000 steps of different particle spacings in the whole calculation process.

Spacing (m)	Real particles	Virtual particles	Total particles (N)	Time (s)/1000 by link-list
0.05	4642	43	4685	405
0.03	18,691	172	18,863	442.5
0.02	60,302	454	60,756	778.75
0.015	13,986	1049	140,911	1432.5
0.01	454,671	3027	457,698	5652.5

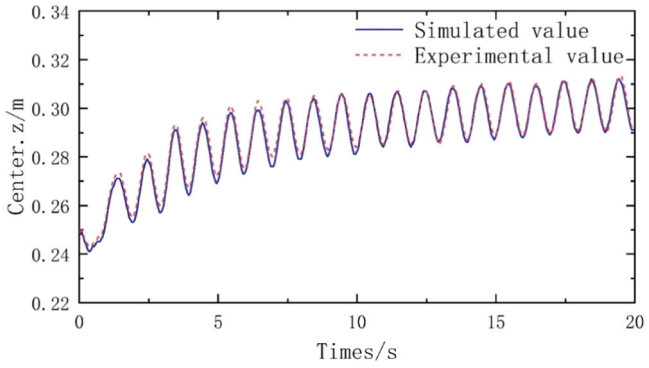

FIGURE 8 | The schematic diagram of the simulated and experimental values of the geometric center change of the front platform of the mooring system is optimized. Figure 8 is to ensure the reliability and applicability of the numerical simulation results, comparing the movement position of the geometric center of the experimental floating platform on the *z*-axis between the experiment and the numerical simulation.

actual experimental value. This shows that numerical simulation has high accuracy in studying the floating performance of floating offshore wind turbine platforms. Numerical simulation. By simulating the same floating conditions, wave conditions, and considering the structural design of the floating offshore wind turbine platform itself, the geometric center change, floating amplitude, and floating speed of the platform can be simulated. This helps evaluate the floating performance and stability of the floating offshore wind turbine platform, optimize the design and structure of the mooring system, and improve its power generation efficiency. Numerical simulation can save experimental cost and time, and improve research efficiency and accuracy. However, to ensure the reliability and applicability of the numerical simulation results, it is necessary to carry out experimental verification in the actual environment.

4.4 | The Influence of Two Mooring Systems on the Stability of the Platform Under Different Waves

The stability of the platform is not only affected by external factors, such as floating conditions, flow conditions, and wave conditions, but also related to the structure and design of its own mooring system. Different mooring system structures and designs may lead to different floating behaviors. The floating amplitude of the platform directly affects the power generation efficiency of the wind turbine. The single-cable mooring system may be challenged because it has only one cable connecting the platform and the anchor point, which is susceptible to lateral and longitudinal forces, resulting in platform shaking or tilting. In contrast, the optimized double-cable mooring system is connected by additional cable strips, which has better wind and wave resistance, can reduce the roll and pitch amplitude of the platform and improve the stability.

4.4.1 | First-Order Irregular Wave Operating Conditions

After the platform is impacted by irregular waves, we can observe the dynamic response of the platform under a single-cable mooring system and a double-cable mooring system through the visual interface. The results show that the double-

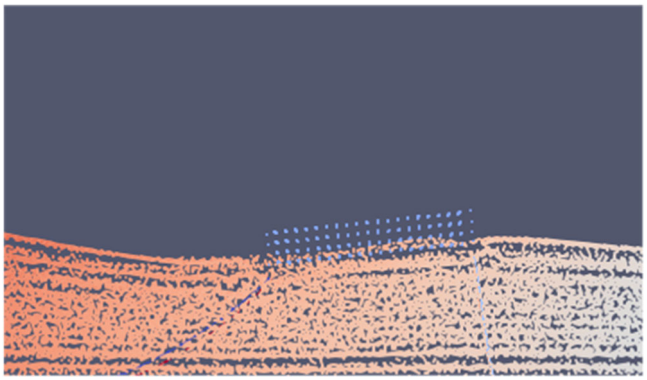

FIGURE 9 | Particle diagram of the single-ropeway mooring system at $t = 15$ s. Figures 9 and 10 show the particle diagram of the dynamic response of the platform at $t = 15$ s after using the visualization software when the platform is subjected to irregular waves. Figure 9 is the single-cable mooring system, and Figure 10 is the double-cable mooring system.

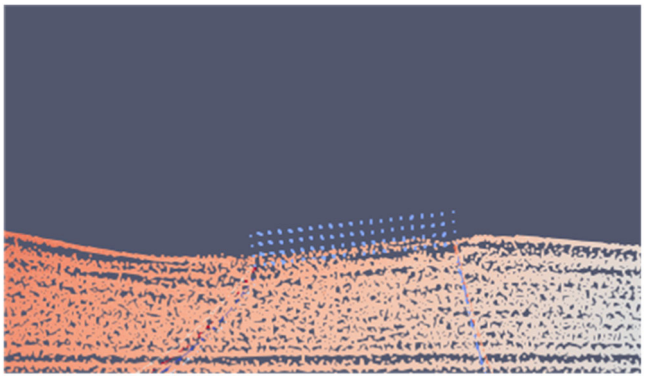

FIGURE 10 | Particle diagram of the double-ropeway mooring system at $t = 15$ s. Figures 9 and 10 show the particle diagram of the dynamic response of the platform at $t = 15$ s after using the visualization software when the platform is subjected to irregular waves. Figure 9 is the single-cable mooring system, and Figure 10 is the double-cable mooring system.

cable mooring system performs better in reducing the amplitude of motion of the platform. Both the translation and rotation are effectively controlled. The optimized mooring system enables the platform to maintain a lower vibration level under the action of waves and plays a better vibration reduction effect. At $t = 15$ s, the visualization of the two mooring systems is shown in Figures 9 and 10.

The influence of the two mooring systems on the geometric center velocity of the platform under irregular wave conditions is shown in Table 3. It can be seen from the data that the double-cable mooring system significantly reduces the speed of the geometric center of the platform in all directions compared with the single-cable mooring system, and further improves the stability and control performance of the platform.

When discussing the vibration problem, the root mean square (RMS) is used as the key parameter of the statistical characteristics of the vibration amplitude. The wave load mentioned in this paper refers to the dynamic force generated by the wave on the platform, which can lead to the translation (horizontal movement) and rotation (rotation) of the structure. The RMS values provided in Table 4 can reflect the dynamic response of the two mooring systems under wave loads. The higher the RMS value, the greater the vibration amplitude. By comparing the RMS value and analyzing the chart data in detail. Figures 11 and 12 show the performance of the single-cable mooring system and the double-cable mooring system in translation and rotation, respectively.

TABLE 3 | Geometric center velocity unit under irregular wave condition (m).

	Single-ropeway mooring system	Double-ropeway mooring system
X	-5.16×10^{-03}	-4.74×10^{-03}
Y	1.264×10^{-04}	8.34×10^{-05}
Z	-2.32×10^{-04}	-3.66×10^{-04}

TABLE 4 | Root mean square unit under irregular wave condition: translation (m) and rotation (deg).

DOF	Single-ropeway mooring system	Double-ropeway mooring system
Sway	0.00139	0.00116
Surge	0.0484	0.0270
Heave	0.0309	0.0281
Roll	0.530	0.274
Pitch	1.44	1.38
Yaw	8.93	7.34

Abbreviation: DOF, degrees of freedom.

It can be seen that under irregular wave conditions, the improvement of the double-cable mooring system on the platform is obvious compared with the single-cable mooring system. In terms of translational motion, the amplitude (RMS) of sway, surge, and heave vibrations decreased by 16.5%, 44.2%, and 9.0%, respectively. Although the improvement of the sway direction is limited, the three degrees of freedom of translation have been significantly improved as a whole. In terms of rotation, the roll, pitch, and yaw deflection amplitudes (RMS) of the platform were reduced by 48.3%, 4.1%, and 17.8%, respectively. Although the improvement of the pitch direction is relatively small, the double-cable mooring system still shows good performance improvement in the three degrees of freedom of rotation. The optimized double-cable mooring system has obvious advantages in platform vibration reduction and stability, which provides more stable and reliable support for platform operation.

4.4.2 | Operating Conditions of Second-Order Regular Wave

After the platform is impacted by regular waves, we can observe the dynamic response of the platform under a single-cable mooring system and a double-cable mooring system through the visual interface. At $t = 15$ s, the visualization of the two mooring systems is shown in Figures 13 and 14.

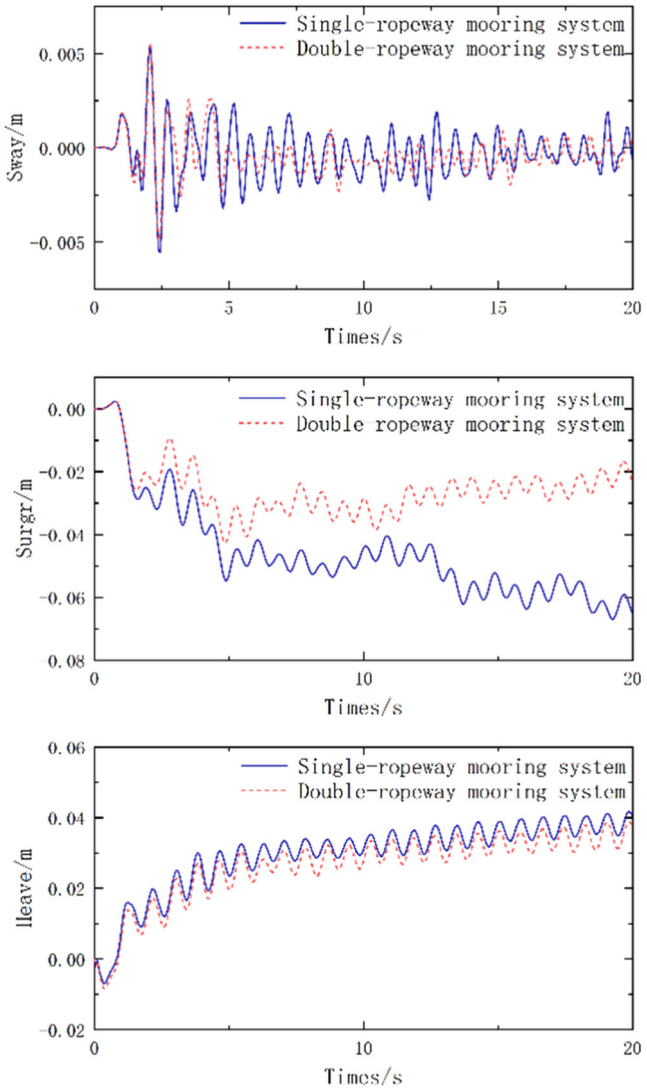

FIGURE 11 | Schematic diagram of translational variation of different mooring systems. Figures 11 and 12 show the comparison of the vibration amplitude data curves of the platform of the single-cable mooring system and the double-cable mooring system in the case of irregular waves in this experiment on six degrees of freedom. Root mean square is used as the key parameter of the statistical characteristics of the vibration amplitude. Figure 11 shows the performance of the single-cable mooring system and the double-cable mooring system in translation, and Figure 12 shows the performance of the single-cable mooring system and the double-cable mooring system in rotation.

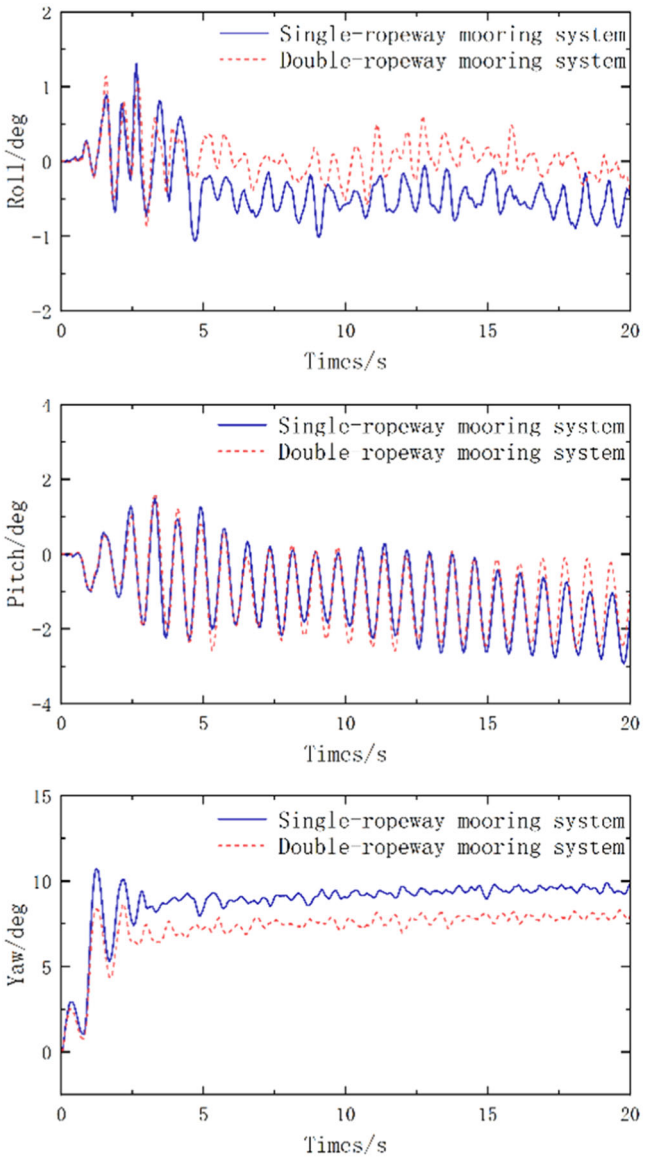

FIGURE 12 | Schematic diagram of rotation change of different mooring systems. Figures 11 and 12 show the comparison of the vibration amplitude data curves of the platform of the single-cable mooring system and the double-cable mooring system in the case of irregular waves in this experiment on six degrees of freedom. Root mean square is used as the key parameter of the statistical characteristics of the vibration amplitude. Figure 11 shows the performance of the single-cable mooring system and the double-cable mooring system in translation, and Figure 12 shows the performance of the single-cable mooring system and the double-cable mooring system in rotation.

The influence of the two mooring systems on the geometric center velocity of the platform under regular wave operating conditions is shown in Table 5. It can be seen from the data that the double-cable mooring system significantly reduces the speed of the geometric center of the platform in all directions compared with the single-cable mooring system, and further improves the stability and control performance of the platform.

The RMS value provided in Table 6 can reflect the dynamic response of the two mooring systems under wave load. The higher the RMS value, the greater the vibration amplitude. By comparing the RMS value and analyzing the chart data in detail. Figures 15 and 16 show the performance of the single-cable mooring system and the double-cable mooring system in translation and rotation, respectively.

It can be seen that under the condition of the regular wave, the improvement of the double-cable mooring system on the platform is obvious compared with the single-cable mooring system. In terms of translational motion, the amplitude (RMS) of sway, surge, and heave vibrations decreased by 5.5%, 38.7%, and 13.1%, respectively. Overall, the three degrees of freedom of translation have been significantly improved. In terms of rotation, the roll, pitch, and yaw deflection amplitudes (RMS) of the platform were

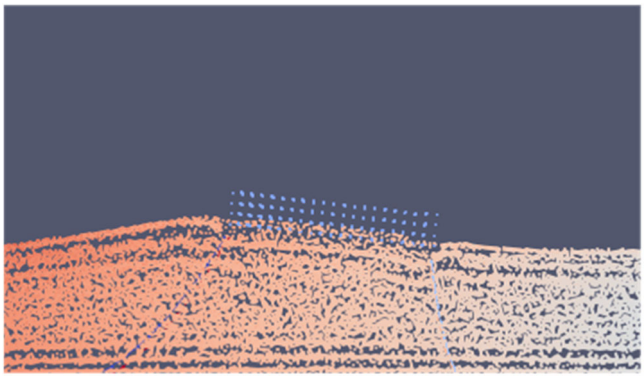

FIGURE 13 | Particle diagram of the single-ropeway mooring system at $t = 15$ s. Figures 13 and 14 show the particle diagram of the dynamic response of the platform at $t = 15$ s after the visualization software is used when the platform is subjected to regular waves. Figure 9 shows the single-ropeway mooring system, and Figure 10 shows the double-ropeway mooring system.

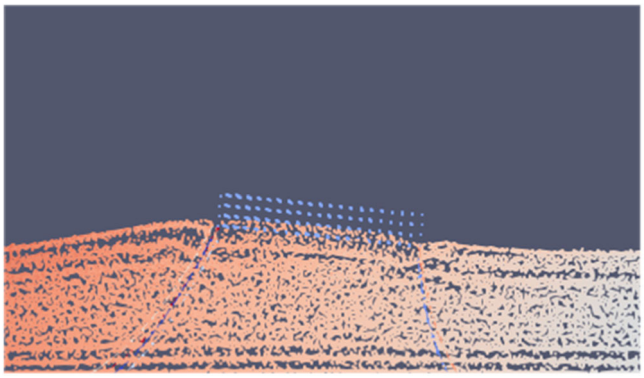

FIGURE 14 | Particle diagram of the double-ropeway mooring system at $t = 15$ s. Figures 13 and 14 show the particle diagram of the dynamic response of the platform at $t = 15$ s after the visualization software is used when the platform is subjected to regular waves. Figure 9 shows the single-ropeway mooring system, and Figure 10 shows the double-ropeway mooring system.

TABLE 5 | Geometric center velocity unit under regular wave condition (m).

	Single-ropeway mooring system	Double-ropeway mooring system
X	-5.29×10^{-03}	-3.89×10^{-03}
Y	-1.6×10^{-03}	-4.55×10^{-06}
Z	-1.21×10^{-03}	-1.01×10^{-03}

reduced by 23.1%, 6.5%, and 17.9%, respectively. The double-cable mooring system still shows good performance improvement in the three degrees of freedom of rotation. The optimized double-cable mooring system has obvious advantages in platform vibration reduction and stability, which provides more stable and reliable support for platform operation. On the whole, the first-order irregular wave and the second-order regular wave are used to simulate the normal operation conditions of different wave actual loads. Compared with the single-cable mooring system, the optimized double-cable mooring system plays an effective optimization

TABLE 6 | Root mean square unit under regular conditions: translation (m) and rotation (deg).

DOF	Single-ropeway mooring system	Double-ropeway mooring system
Sway	0.00146	0.00138
Surge	0.0652	0.0400
Heave	0.0427	0.0371
Roll	1.08	0.830
Pitch	2.00	1.87
Yaw	9.37	7.69

Abbreviation: DOF, degrees of freedom.

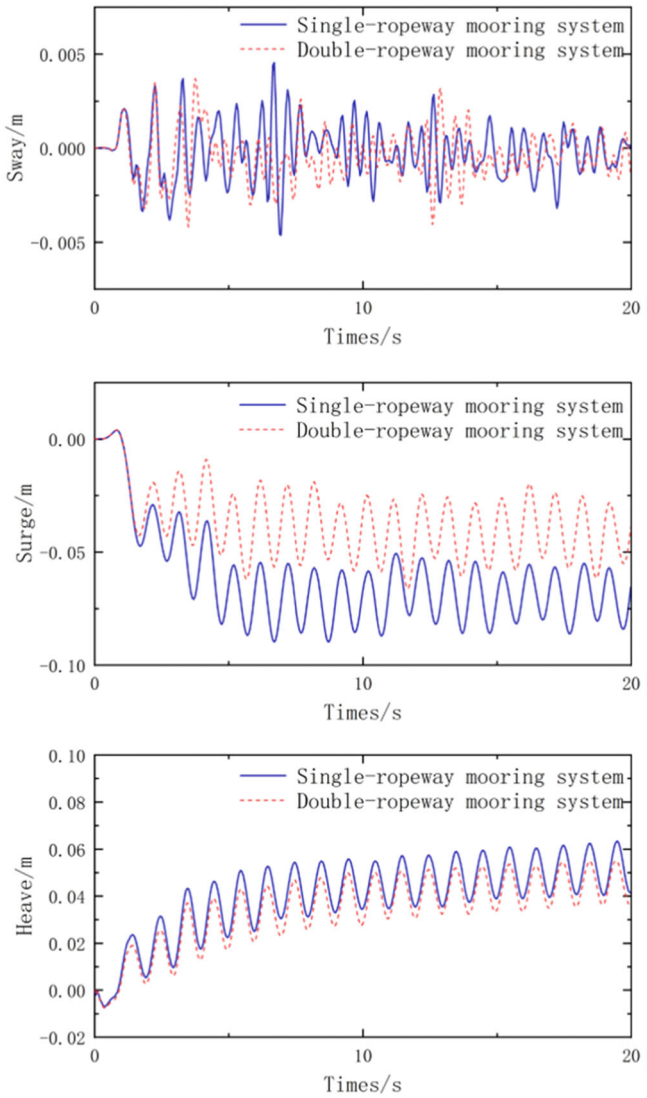

FIGURE 15 | Schematic diagram of translational variation of different mooring systems. Figures 15 and 16 show the comparison of vibration amplitude data curves on six degrees of freedom of the platform of the single-cable mooring system and the double-cable mooring system in the case of regular waves. Root mean square is used as the key parameter of the statistical characteristics of vibration amplitude. Figure 15 shows the performance of the single-cable mooring system and the double-cable mooring system in translation, and Figure 16 shows the performance of the single-cable mooring system and the double-cable mooring system in rotation.

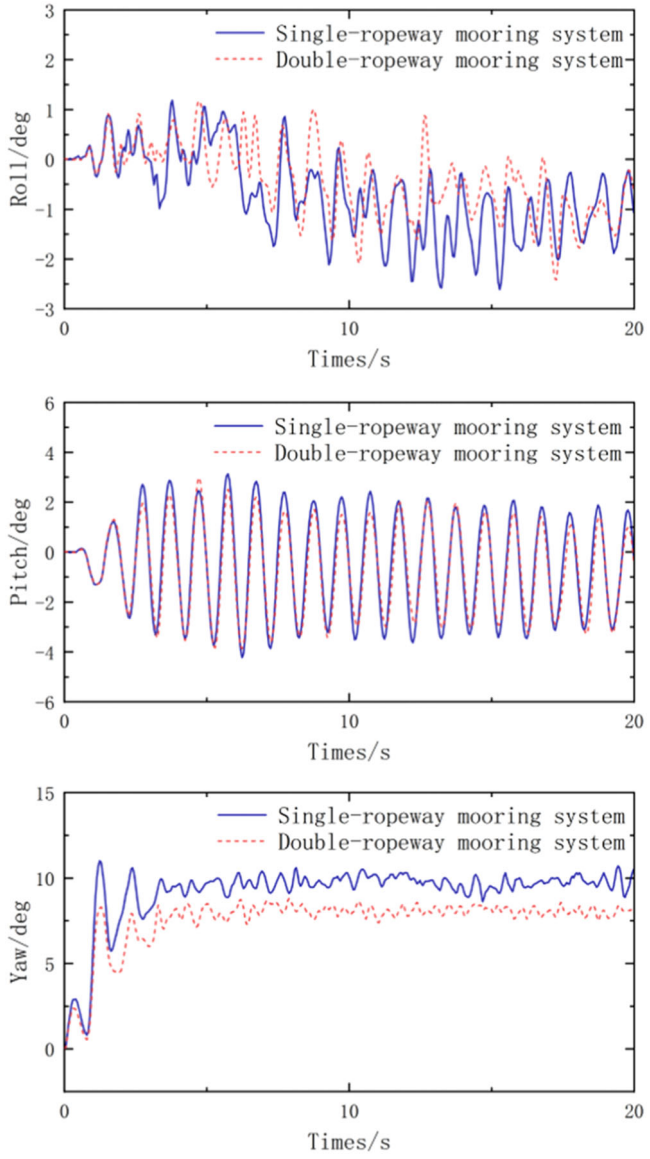

FIGURE 16 | Schematic diagram of rotation change of different mooring systems. Figures 15 and 16 show the comparison of vibration amplitude data curves on six degrees of freedom of the platform of the single-cable mooring system and the double-cable mooring system in the case of regular waves. Root mean square is used as the key parameter of the statistical characteristics of vibration amplitude. Figure 15 shows the performance of the single-cable mooring system and the double-cable mooring system in translation, and Figure 16 shows the performance of the single-cable mooring system and the double-cable mooring system in rotation.

role in the vibration reduction performance of the platform. By effectively controlling and mitigating the vibration of the platform, the double-cable mooring system improves the stability and comfort of the platform and provides a safer and more reliable environment for the operation of the platform.

5 | Conclusion

In this paper, an innovative mooring system for floating offshore wind turbines is proposed, and the SPH method is used to simulate the improved mooring system. The improved double-cableway mooring system is compared and analyzed with the traditional single-cableway mooring system. Through numerical simulation, the dynamic response of the platform under different ocean conditions is studied, and the trajectory of the geometric center of the platform, the velocity of the geometric center, and the six-degrees-of-freedom motion are analyzed. Especially in terms of suppressing platform vibration, the dual-cableway mooring system shows significant advantages. The results show that the double-ropeway mooring system not only effectively reduces the pitch, roll and heave motion of the platform, but also provides a redundancy guarantee for the mooring system in the complex wind and wave environment and prolongs the service life of the platform. By optimizing the layout and force distribution of the mooring line, the double-cableway mooring system can better disperse the external environmental load, effectively balance the movement of the platform in all directions, enhance the wind and wave resistance of the platform, and improve the stability and efficiency of the generator. Under the condition of strong winds and waves, the double-cableway mooring system can quickly respond to and suppress large-scale motion, significantly reduce the dynamic stress and vibration amplitude of the platform, and ensure the safety and operation reliability of power generation equipment.

This paper not only provides the theoretical basis and numerical support for the mooring system design of floating offshore wind turbine platform, but also makes important contributions to technological innovation in this field. This study demonstrates the great potential of the dual-ropeway mooring system in improving the stability and vibration reduction performance of the floating wind power generation platform, which is expected to promote the development of offshore wind power generation technology, especially for the construction of far-reaching sea wind electric field in the future. The application of this new mooring system will help improve the power generation efficiency of floating wind power generation, reduce maintenance costs, and promote further breakthroughs in the sustainable development of energy in the wind power industry. To further improve the accuracy and practicality of the research, future work plans include more quantitative comparisons. These comparisons will use data from a wider range of laboratory experiments and field tests to ensure that the simulation results can maintain a high degree of consistency and reliability under various operating conditions. In addition, future research will explore more factors that affect the dynamic response of wind turbine platforms, such as changes in the marine environment, wind speed and wave dynamics, so as to provide a more comprehensive theoretical and practical basis for the design and optimization of mooring systems for floating offshore wind turbines. Through these in-depth studies, the economy and reliability of floating wind power generation technology can be further improved to contribute to sustainable energy development.

References

1. J. Li, G. Wang, Z. Li, S. Yang, W. T. Chong, and X. Xiang, "A Review on Development of Offshore Wind Energy Conversion System," *International Journal of Energy Research* 44, no. 12 (2020): 9283–9297, https://doi.org/10.1002/er.5751.

2. M. D. Esteban, J. J. Diez, J. S. López, and V. Negro, "Why Offshore Wind Energy?," *Renewable Energy* 36, no. 2 (2011): 444–450, https://doi.org/10.1016/j.renene.2010.07.009.

3. J. J. Monaghan, "Simulating Free Surface Flows With SPH," *Journal of Computational Physics* 110, no. 2 (1994): 399–406, https://doi.org/10.1006/jcph.1994.1034.

4. B. Ren, M. He, Y. Li, and P. Dong, "Application of Smoothed Particle Hydrodynamics for Modeling the Wave-Moored Floating Breakwater Interaction," *Applied Ocean Research* 67 (2017): 277–290, https://doi.org/10.1016/j.apor.2017.07.011.

5. J. M. Domínguez, A. J. C. Crespo, M. Hall, et al., "SPH Simulation of Floating Structures With Moorings," *Coastal Engineering* 153 (2019): 103560, https://doi.org/10.1016/j.coastaleng.2019.103560.

6. M. H. Aslami, B. D. Rogers, P. K. Stansby, and A. Bottacin-Busolin, "Simulation of Floating Debris in SPH Shallow Water Flow Model With Tsunami Application," *Advances in Water Resources* 171 (2023): 104363, https://doi.org/10.1016/j.advwatres.2022.104363.

7. S. Capasso, B. Tagliafierro, S. Mancini, et al., "Regular Wave Seakeeping Analysis of a Planing Hull by Smoothed Particle Hydrodynamics: A Comprehensive Validation," *Journal of Marine Science and Engineering* 11, no. 4 (2023): 700.

8. A. Barreiro, A. J. C. Crespo, J. M. Dominguez, O. Garcia-Feal, I. Zabala, and M. Gomez-Gesteira, "Quasi-Static Mooring Solver Implemented in SPH," *Journal of Ocean Engineering and Marine Energy* 2 (2016): 381–396, https://doi.org/10.1007/s40722-016-0061-7.

9. B. Tagliafierro, M. Karimirad, I. Martínez-Estévez, J. M. Domínguez, G. Viccione, and A. J. C. Crespo, "Numerical Assessment of a Tension-Leg Platform Wind Turbine in Intermediate Water Using the Smoothed Particle Hydrodynamics Method," *Energies* 15, no. 11 (2022): 3993, https://doi.org/10.3390/en15113993.

10. B. Tagliafierro, I. Martínez-Estévez, J. M. Domínguez, et al., "A Numerical Study of a Taut-Moored Point-Absorber Wave Energy Converter With a Linear Power Take-Off System Under Extreme Wave Conditions," *Applied Energy* 311 (2022): 118629, https://doi.org/10.1016/j.apenergy.2022.118629.

11. B. Tagliafierro, M. Karimirad, C. Altomare, et al., "Numerical Validations and Investigation of a Semi-Submersible Floating Offshore Wind Turbine Platform Interacting With Ocean Waves Using an SPH Framework," *Applied Ocean Research* 141 (2023): 103757, https://doi.org/10.1016/j.apor.2023.103757.

12. N. Quartier, *Numerical Modelling of Moored Floating Structures and Energy Devices Using a Smoothed Particle Hydrodynamics-Based Solver* (Ghent, Belgium: Ghent University, 2023).

13. P. W. Cleary and M. Rudman, "Extreme Wave Interaction With a Floating Oil Rig: Prediction Using SPH," *Progress in Computational Fluid Dynamics, an International Journal* 9, no. 6–7 (2009): 332–344, https://doi.org/10.1504/PCFD.2009.027364.

14. A. Colmenar-Santos, J. Perera-Perez, D. Borge-Diez, and C. dePalacio-Rodríguez, "Offshore Wind Energy: A Review of the Current Status, Challenges and Future Development in Spain," *Renewable and Sustainable Energy Reviews* 64 (2016): 1–18, https://doi.org/10.1016/j.rser.2016.05.087.

15. H. Díaz and C. Guedes Soares, "Review of the Current Status, Technology and Future Trends of Offshore Wind Farms," *Ocean Engineering* 209 (2020): 107381, https://doi.org/10.1016/j.oceaneng.2020.107381.

16. L. B. Lucy, "A Numerical Approach to the Testing of the Fission Hypothesis," *Astronomical Journal* 82 (1977): 1013–1024, https://doi.org/10.1086/112164.

17. R. A. Gingold and J. J. Monaghan, "Smoothed Particle Hydrodynamics: Theory and Application to Non-Spherical Stars," *Monthly Notices of the Royal Astronomical Society* 181, no. 3 (1977): 375–389, https://doi.org/10.1093/mnras/181.3.37.

18. S. J. Lind, B. D. Rogers, and P. K. Stansby, "Review of Smoothed Particle Hydrodynamics: Towards Converged Lagrangian Flow Modelling," *Proceedings of the Royal Society A* 476, no. 2241 (2020): 20190801, https://doi.org/10.1098/rspa.2019.0801.

19. Z. Liu and Y. Wang, "Numerical Studies of Submerged Moored Box-Type Floating Breakwaters With Different Shapes of Cross-Sections Using SPH," *Coastal Engineering* 158 (2020): 103687, https://doi.org/10.1016/j.coastaleng.2020.103687.

20. Z. Tan, P. N. Sun, N. N. Liu, Z. Li, H. G. Lyu, and R. H. Zhu, "SPH Simulation and Experimental Validation of the Dynamic Response of Floating Offshore Wind Turbines in Waves," *Renewable Energy* 205 (2023): 393–409, https://doi.org/10.1016/j.renene.2023.01.081.

21. M. B. Liu and G. R. Liu, "Smoothed Particle Hydrodynamics (SPH): An Overview and Recent Developments," *Archives of Computational Methods in Engineering* 17 (2010): 25–76, https://doi.org/10.1007/s11831-010-9040-7.

22. J. J. Monaghan, "Smoothed Particle Hydrodynamics," *Annual Review of Astronomy and Astrophysics* 30, no. A93-25826 09-90 (1992): 543–574, https://doi.org/10.1146/annurev.aa.30.090192.002551.

23. A. Muta and P. Ramachandran, "Efficient and Accurate Adaptive Resolution for Weakly-Compressible SPH," *Computer Methods in Applied Mechanics and Engineering* 395 (2022): 115019, https://doi.org/10.1016/j.cma.2022.115019.

24. J. J. Monaghan, "Smoothed Particle Hydrodynamics and Its Diverse Applications," *Annual Review of Fluid Mechanics* 44 (2012): 323–346, https://doi.org/10.1146/annurev-fluid-120710-101220.

25. G. R. Liu and M. B. Liu, "Smoothed Particle Hydrodynamics: A Meshfree Particle Method," *World Scientific* (2003), https://doi.org/10.1007/s00466-004-0573-1.

26. S. Marrone, A. Di Mascio, and D. Le Touzé, "Coupling of Smoothed Particle Hydrodynamics With Finite Volume Method for Free-Surface Flows," *Journal of Computational Physics* 310 (2016): 161–180, https://doi.org/10.1016/j.jcp.2015.11.059.

27. C. Altomare, A. J. C. Crespo, B. D. Rogers, J. M. Dominguez, X. Gironella, and M. Gómez-Gesteira, "Numerical Modelling of Armour Block Sea Breakwater With Smoothed Particle Hydrodynamics," *Computers & Structures* 130 (2014): 34–45, https://doi.org/10.1016/j.compstruc.2013.10.011.

28. C. Altomare, A. J. C. Crespo, J. M. Domínguez, M. Gómez-Gesteira, T. Suzuki, and T. Verwaest, "Applicability of Smoothed Particle Hydrodynamics for Estimation of Sea Wave Impact on Coastal Structures," *Coastal Engineering* 96 (2015): 1–12, https://doi.org/10.1016/j.coastaleng.2014.11.001.

29. S. L. Peng, M. B. Liu, and M. B. Liu, *Numerical Simulation of Ballast Water by SPH Method*, (Singapore: World Scientific Publishing Co Pte Ltd.) https://doi.org/10.1142/S0219876212400026.

30. B. Bouscasse, A. Colagrossi, S. Marrone, and M. Antuono, "Nonlinear Water Wave Interaction With Floating Bodies in SPH," *Journal of Fluids and Structures* 42 (2013): 112–129, https://doi.org/10.1016/j.jfluidstructs.2013.05.010.

31. A. J. Cabrera Crespo, R. Gómez-Gesteira, and R. A. Dalrymple, "Boundary Conditions Generated by Dynamic Particles in SPH Methods [J]," *Computers, Materials, & Continua* (2007), https://doi.org/10.3970/cmc.2007.005.173.

32. K.-T. Ma, Y. Luo, T. Kwan, and Y. Wu, *Mooring System Engineering for Offshore Structures* (Houston, Texas, USA: Gulf Professional Publishing, 2019).

33. D. Stewart, "A Platform With Six Degrees of Freedom," *Proceedings of the Institution of Mechanical Engineers* 180, no. 1 (1965): 371–386, https://doi.org/10.1243/PIME_PROC_1965_180_029_02.

34. D. Weibo, "Numerical Study of Inter-Floating Platform Mooring Systems Based on the SPH Method," in *Proceedings at the 15th*

International Conference of Computational Methods (ICCM2024), July 15–18, 2024, eds. G. Liu and V.-H. Nguyen (ScienTech Publisher, 2024).

35. J. Liu, P. Jiao, and Y. Xu, "Research on Oil Boom Performance Based on Smoothed Particle Hydrodynamics Method," *PLoS ONE* 18, no. 7 (2023): e0289276, https://doi.org/10.1371/journal.pone.0289276.

36. R. Fatehi and M. T. Manzari, "A Consistent and Fast Weakly Compressible Smoothed Particle Hydrodynamics With a New Wall Boundary Condition," *International Journal for Numerical Methods in Fluids* 68, no. 7 (2012): 905–921, https://doi.org/10.1002/fld.2586.

37. Z. Mao, G. R. Liu, and X. Dong, "A Comprehensive Study on the Parameters Setting in Smoothed Particle Hydrodynamics (SPH) Method Applied to Hydrodynamics Problems," *Computers and Geotechnics* 92 (2017): 77–95.